# Detection of gaseous species during KCl-induced high-temperature corrosion by means of CPFAAS and CI-APi-TOF

Juho LEHMUSTO[1)], Miska OLIN[2)], Jan VILJANEN[3)], Joni KALLIOKOSKI[2)], Fanni MYLLÄRI[2)], Juha TOIVONEN[3)], Miikka DAL MASO[2)], Leena HUPA[1)]

1) Laboratory of Inorganic Chemistry, Johan Gadolin Process Chemistry Centre, Abo Akademi University, Turku, Finland

[2)] Aerosol Physics Laboratory, Physics Unit, Tampere University, Tampere, Finland

[3)] Photonics Laboratory, Physics Unit, Tampere University, Tampere, Finland

**Correspondence**

Juho Lehmusto, Laboratory of Inorganic Chemistry, Johan Gadolin Process Chemistry Centre, Abo Akademi University, Turku, Finland

Email: juho.lehmusto@abo.fi

**Keywords:**

High-temperature corrosion, gaseous KCl, HCl formation, CPFAAS, CI-APi-TOF

**Abstract**

Two different analytical approaches - collinear photofragmentation and atomic absorption spectroscopy (CPFAAS) and chemical ionization atmospheric pressure interface time-of-flight mass spectrometer (CI-APi-TOF) were applied to detect and identify online gaseous KOH and HCl formed in the addressed high-temperature reactions. Samples of pure KCl, KCl+Cr, KCl+Fe, and KCl+316L were studied at 550 °C under dry and humid conditions with varying oxygen concentrations. The goal was to shed more light on the gas-phase chemistry during KCl-induced corrosion under conditions relevant to biomass combustion. CI-APi-TOF proved to be a valuable tool for high-temperature corrosion studies: HCl was identified to have formed during the reactions under humid conditions. On the contrary, despite the known sensitivity of CPFAAS, the formation of KOH could not be verified in any of the performed measurements.

## 1 Introduction

Dwindling reservoirs of fossil fuels together with the negative impact of coal combustion on climate change through $CO_2$ emissions have increased interest in alternative fuels for power production. Renewable fuels such as biomass are considered as a part of the solution, mainly due to their $CO_2$-neutrality, availability, and tax relief-based profitableness. However, due to the heterogeneous nature of the feedstock, the combustion of biomass poses certain challenges compared to the relatively homogeneous fossil fuels. One of the main concerns is the presence of potassium and chlorine in larger quantities, which are released into the flue gas during combustion [1,2]. Potassium and chlorine can react to potassium chloride (KCl), either in the gas phase or in the deposits condensed on the heat-transfer surfaces. The formed potassium chloride is known to be detrimental and its corrosivity has been reported in several publications both in the lab-scale [e.g. 3] and in running boilers [e.g. 4]. Despite the extensive research, the reaction mechanism between KCl and the protective oxide on the alloy surface is not yet fully understood. This holds true particularly well in terms of gaseous species. At present, it is

generally accepted that both under dry and humid conditions, the reaction initiates through potassium chromate ($K_2CrO_4$) formation, depleting the protective oxide in chromium (R1a,b). The simultaneously increasing porosity of the protective oxide followed by the loss of its protective properties will accelerate the migration of oxygen and corrosive species through the oxide to the oxide/alloy interface, eventually leading to breakaway corrosion.

$$8KCl(s,g) + 2Cr_2O_3(s) + 5O_2(g) \rightarrow 4K_2CrO_4(s) + 4Cl_2(g) \quad \text{(R1a)}$$

$$8KCl(s,g) + 2Cr_2O_3(s) + 3O_2(g) + 4H_2O(g) \rightarrow 4K_2CrO_4(s) + 8HCl(g) \quad \text{(R1b)}$$

The environments relevant to biomass combustion always contain humidity, making Reaction (R1a) less likely to occur. Instead, the formation of $K_2CrO_4$ and HCl according to Reaction (R1b) is plausible and thus forms the identified $K_2CrO_4$ [5]. Interestingly, as the formation of HCl has not been addressed before, the reaction mechanism (R1b) has not been completely verified. Another uncertainty lies in the progression of the reaction; $K_2CrO_4$ is considered an intermediate, which reacts further over time. So far, the decomposition of $K_2CrO_4$ under humid conditions has been proposed to take place via electrochemical reduction (R2) [6]. This reaction yields molten potassium hydroxide (KOH), which can volatilize in typical temperatures in the boiler [7]. KOH can also form in a direct reaction between KCl and water vapor, producing also HCl [8] or chloride ions [9].

$$K_2CrO_4(s) + 3e^- + H_2O(g) \leftrightarrow KOH(l) + \tfrac{1}{2}Cr_2O_3(s) \quad \text{(R2)}$$

To complement the reaction chain addressing KCl-induced high-temperature corrosion, more information regarding the gaseous species involved in the reaction destroying the protective properties of the $Cr_2O_3$ scale is required. For this, new approaches should be considered.

Laser spectroscopy enables rapid non-intrusive in-situ monitoring of high-temperature gas-phase chemistry. Multiple laser-based methods, such as tunable diode laser absorption spectroscopy (TDLAS) [10] and laser-induced fluorescence (LIF) [11] have been introduced for gas-phase reaction studies in combustion applications. Also, alkali species in high-temperature environments have been under inspection using laser methods. Photofragmentation and laser-induced fluorescence (PF-LIF) is extensively used for the detection of alkali chlorides and hydroxides [12-14]. This method allows sensitive detection and imaging of alkali species but, however, is incapable to distinguish between e.g. KCl and KOH but relies on equilibrium calculations when concentrations of individual molecules are given. Differential optical absorption spectroscopy (DOAS) is capable of providing sensitive online monitoring of alkali species [15-17]. As it, similarly to PF-LIF, relies on alkali molecule absorption in ultraviolet (UV) region of the electromagnetic spectrum, DOAS suffers from spectral overlapping of alkali species' absorption bands causing interference in collected signal [18]. A recently introduced technique called collinear photofragmentation and atomic absorption spectroscopy (CPFAAS) has shown the ability for sensitive molecule specific detection of alkali species providing sub-ppm detection limits [19,20]. CPFAAS is based on UV photofragmentation of precursor molecule and fragment detection. A UV laser pulse excites the molecule into a dissociative state producing fragments that are detected using direct absorption measurement with a continuous wave (CW) probe laser. Choice of the fragmenting laser and the probe laser wavelengths allow

selective detection of alkali chlorides and hydroxides [20]. Therefore, CPFAAS is chosen to be used in this work for KOH detection in the gas phase during corrosion reaction.

Analyzing gaseous HCl optically, e.g. by using a laser-based cavity ring-down spectroscopy (CRDS), can provide HCl in the lowest detectable concentrations down to ppt level [21]. However, HCl is challenging to identify with CPFAAS, the other optical measurement involved in this study and due to the potential interference of any unburned particulate matter with the optical detection of HCl, also mass spectrometry was used to detect HCl in this study. In some studies, chemical ionization mass spectrometry (CIMS) has been used to detect HCl concentrations in the atmosphere (e.g. [22]). CIMS is based on selective ionization of the sample using a specific reagent ion after which the resulting ions are classified according to their mass-to-charge ratios (*m*/*z*). Acetate ions [22] and sulfur hexafluoride ions [23] have been used as the reagent ions to detect HCl using CIMS. In this study, a high-resolution CIMS, known as the atmospheric pressure interface time-of-flight mass spectrometer (CI-APi-TOF) [24,25], was applied for the detection of HCl. CI-APi-TOF has recently been used in several atmospheric studies to detect very low concentrations of gaseous species [24]. However, to the best of our knowledge, CI-APi-TOF has never before been used for analyses addressing high-temperature reactions. One of the most commonly used reagent ion with CI-APi-TOF is the nitrate ion ($NO_3^-$) [26] which selectively ionizes neutral acids having higher acid strengths compared to nitric acid ($HNO_3$) via the following proton transfer and ligand switching reactions:

$$HA + (HNO_3)_{n\in\mathbb{N}} \cdot NO_3^- \rightarrow A^- + (HNO_3)_{n\in\mathbb{N}} \cdot HNO_3 \quad \text{(R3a)}$$

$$HA + (HNO_3)_{n\in\mathbb{N}} \cdot NO_3^- \rightarrow HNO_3 \cdot A^- + (HNO_3)_{n\in\mathbb{N}} \quad \text{(R3b)}$$

where HA is the acid and $A^-$ its conjugate base. Acids having higher acid strengths compared to $HNO_3$ include, e.g., sulfuric acid ($H_2SO_4$) and hydrochloric acid (HCl). Traditionally, $H_2SO_4$ has been one of the most commonly measured gaseous species using CI-APi-TOF because this method is superior to any other method in measuring trace level concentrations of $H_2SO_4$ in the atmosphere. The lowest measurable $H_2SO_4$ concentrations are in ppq level [24]; thus, it is expected that also HCl can be measured in very low concentrations using CI-APi-TOF.

The detection of HCl with nitrate ion-based CI-APi-TOF was assumed to be equal to the detection of $H_2SO_4$ because both the acids have higher acid strengths compared to $HNO_3$. Hence, the following reactions would apply:

$$HCl + (HNO_3)_{n\in\mathbb{N}} \cdot NO_3^- \rightarrow Cl^- + (HNO_3)_{n\in\mathbb{N}} \cdot HNO_3 \quad \text{(R4a)}$$

$$HCl + (HNO_3)_{n\in\mathbb{N}} \cdot NO_3^- \rightarrow HNO_3 \cdot Cl^- + (HNO_3)_{n\in\mathbb{N}} \quad \text{(R4b)}$$

The aim of the research is to explore whether the two different analytical approaches; collinear photofragmentation and atomic absorption spectroscopy (CPFAAS) or chemical ionization atmospheric pressure interface time-of-flight mass spectrometer (CI-APi-TOF) can be used for online detection of high-temperature corrosion reactions. The focus lies on the identification of gaseous species formed in a KCl-induced corrosion reaction under conditions relevant to biomass combustion.

## 2 Experimental

The corrosion mechanisms were studied using powder samples consisting of KCl (Merck *zur Analyze*) mixed with either chromium (Alfa Aesar 99%, average particle size 149 μm), iron (Merck Emsure 99.5%, average particle size 10 μm), or 316L (Sandvik, average particle size 30 – 90 μm). The pure metals chromium and iron were used to simplify the analysis of the gaseous phase, whereas the alloy 316L was chosen to represent typical stainless steel used in industrial applications where a good corrosion resistance at elevated temperatures is required. The main elements of 316L were measured to be Fe (62 at.%), Cr (20 at.%), and Ni (12 at.%). Also smaller amounts of Mn, Mo, and Si were detected. Prior to the exposures, the powders were weighed and mixed in a KCl-to-metal molar ratio of 1:1 before placing the sample in a 10 cm long alumina combustion boat (AlSint, Haldenwanger). The experiments and used instruments are described in greater detail later in the text and summarized here in Table 1. For the CI-APi-TOF measurements, a temperature of 550 °C was chosen, because it represents well the current surface temperature of a superheater tube in a biomass-fired power plant and it does not damage the instrument.

**Table 1.** Experiments carried out in the present study.

The photofragmentation process was initiated by using the third harmonic of an Nd:YAG pulsed laser (Ultra Big Sky series, Quantel) emitting at 355 nm with a pulse duration of 5 ns at a repetition rate of 10 Hz (Figure 1.). The diameter of the fragmenting beam was 2 mm and pulse energies varied between 30 μJ and 125 μJ. Fragmenting laser pulse energy was varied to avoid any interference signal from evaporated KCl. According to the equilibrium calculations, the KCl concentration in the gas phase varies from 0.1 ppm to 150 ppm at temperatures of 550 °C and 750 °C, respectively. The atomic potassium fragments were monitored using narrow-linewidth distributed feedback diode laser (Nanoplus GmbH) that was tuned to potassium D2 absorption line at 766.5 nm using a reference potassium cell (SC-K-19 75-Q-W, Photonics Technologies). The probe beam was aligned collinearly with the fragmenting beam within the desired measurement volume using dichroic mirrors. The temporal intensity of probe beam transmission was recorded with an amplified photodetector (PDA10A, Thorlabs) that was connected to 12-bit oscilloscope (HDO6054, LeCroy).

**Figure 1.** A schematic representation of the CPFAAS measurement arrangement used for KOH detection: dichroic mirror, DM; energy meter, EM; photodetector, PD.

The laser beams were aligned to pass through a 60 cm long quartz tube furnace propagating 2 mm above the combustion boat with the sample. The exposures were performed at 550, 650, and 750 °C and contained only the KCl+Cr mixture. To quantify the amount of KOH that formed in the absence of chromium, the exposures were first carried out with pure KCl in an atmosphere with varying oxygen content (0, 1, 5, 10, and 20 vol.%) both under dry and humid (30 vol.% $H_2O$) conditions. The KCl+Cr mixture was studied under the same conditions. The gas composition in the reactor was adjusted with a mass flow controller (5850S, Brooks Instruments) diluting dry synthetic air with nitrogen. Moisture content in the reactor was

controlled using water vapor seeding to the reactor input gas. To amplify the KOH signal, the laser measurements were performed under stagnant conditions. Prior to the laser pulses, the reactor was flushed with the atmosphere in question for five minutes, after which the gas flow was turned off.

Nitrate ion-based CI-APi-TOF was used to measure HCl as $Cl^-$ and $HNO_3 \cdot Cl^-$ ions. The hot gas sample from the oven was diluted with 8 slpm of air at room temperature using a mass flow controller. The sample flow rate to CI-APi-TOF was 10 slpm, which corresponds to the dilution ratio of 5. Losses of HCl onto the walls of the sampling lines between the oven and the inlet of the APi-TOF may occur, but not in a scale that would distort the results. So far, concentration calibration has been performed for $H_2SO_4$ only [27]. Therefore, the absolute concentrations of HCl cannot be reliably reported. To measure the HCl formation originating from residual water or from the direct reaction between KCl and $H_2O$, pure KCl was exposed to synthetic air (20 vol.% $O_2$ + 80 vol.% $N_2$) and to synthetic air with water vapor contents of 10, 20, and 30 vol.%. The mixtures KCl+Cr, KCl+Fe, and KCl+316L were studied under two conditions; i) in synthetic air with a water vapor content of 30 vol.% and ii) in an atmosphere containing 30 vol.% $H_2O$, $N_2$ as balance gas and 0, 1, 5, 10, or 20 vol.% $O_2$. The latter environment was studied to clarify the potential oxygen dependence of HCl formation.

CI-APi-TOF measured times-of-flight for masses between 2 and 776 Th in 1 s time resolution. The dwell time for the gas sample from the oven to the CI-APi-TOF instrument was between 0.2 and 0.5 seconds., giving a very rapid response. Times-of-flight were converted to mass-to-charge ratios by mass calibration using the exact masses of four compounds known to exist in spectra measured with nitrate ion-based CI-APi-TOF: $NO_2^-$ (45.9935 Th), $NO_3^-$ (61.9884 Th), $HNO_3 \cdot NO_3^-$ (124.9840 Th), and $C_6H_5NO_3 \cdot NO_3^-$ (201.0153 Th).

After the measurements, some of the sample mixtures were studied using scanning electron microscopy and energy-dispersive X-ray spectroscopy (SEM-EDX) with a focus on the chemical compositions of the reacted mixtures. The microscope (SEM-LEO Gemini 1530 with a NORAN Vantage X-ray analyzing system manufactured by Thermo Fisher Scientific) was operated in secondary and backscattering electron modes at an accelerating voltage of 15 kV for the EDX analyses and for imaging with an aperture size of 60 me and a beam current of 1 nA.

## 3 Results and discussion

### 3.1 CPFAAS

The limit of detection (LOD) for KOH was estimated to be 5 ppb provided that a change of 0.5% in the transmission can be detected [28]. The key factor affecting the LOD was the presence of KCl in the gas phase as it sublimated from the sample holder. The vapor pressure of KCl in Torr, p(KCl) can be calculated with Equation (1), where T is the temperature in Kelvin [29]. At the test temperatures of 550, 650, and 750 °C, the calculated p(KCl) were, $1.6 \cdot 10^{-10}$, $3.4 \cdot 10^{-9}$, and $4.3 \cdot 10^{-18}$ Torr, respectively. The absorption cross section of KCl at 355 nm is orders of magnitude lower than that of KOH [18,20]. However, as the detection system was tuned to be as sensitive as possible by using a small beam diameter, KCl caused interferences when high laser pulse energy was used. To avoid interferences caused by KCl, the use of lower

fragmenting laser pulses was required, compromising the detection limit. To demonstrate the sensitivity of the detection system, typical signals from pure KCl at 750 °C and from the KCl+Cr reaction mixture at 650 °C are presented in Figure 2. Both samples were measured with 120 μJ laser pulse energy and the detected intensities are presented as functions of time.

$$log_{10}p(KCl) = -8.0224 - 9.3722 \times \frac{10^3}{T} + 6.4641 log_{10}T - 3.1639 \times 10^{-3}T + 3.32745 \times 10^{-7}T^2 \quad (1)$$

**Figure 2.** A typical signal obtained during corrosion reaction (gray line). The KOH signal was collected when a KCl+Cr mixture was exposed at 650 °C in the presence of 30 vol.% water vapor. As a comparison, a typical KCl signal collected with 120 μJ fragmenting laser pulse energy is also presented (black line). The KCl signal was measured from a pure KCl sample exposed under dry conditions at 750 °C in $N_2$.

Although the method is sensitive and able to measure very low concentrations, no KOH could be verified in any of the performed measurements. When measuring gaseous species formed during biomass combustion, KOH has been identified at temperatures above 1100 K. It might also form in the gas-phase reaction between KCl and $H_2O$ at around 1350 K [30]. The lower temperatures used in the present study might partly explain, why KOH did not form directly from KCl. In addition to the temperature, the formation of KOH has been reported to depend also on the potassium-to-chlorine ratio in the gas phase [8]. When the potassium-to-chlorine ratio was higher than one, gaseous KOH was stable at temperatures prevailing at superheater surfaces. Since the potassium-to-chlorine ratio was not measured in the present study, its impact on the KOH formation could not be verified and is thus not discussed further.

The elemental composition of the KCl+Cr mixture was studied with SEM after the experiments. A compound with a K:Cr:O-ratio of 1:2:4 indicated the formation of potassium chromate ($K_2CrO_4$). The same compound which has previously been identified with an X-ray powder diffractometer [31] for experiments performed under conditions similar to the ones used in the present study. Potassium chromate is an intermediate, whose amount decreases over time, thus indicating that it reacts further or decomposes. Despite $K_2CrO_4$ was formed in the present study, its gradual later decomposition did not produce gaseous KOH as suggested previously [32].

In the presence of pure iron and 316L steel, any KOH that forms can react with it further to solid potassium ferrite ($K_2Fe_2O_4$). However, no $K_2Fe_2O_4$ could be identified. The reaction kinetics of potassium in the gas phase was studied using CPFAAS by fragmenting KCl molecules with a pulsed laser emitting at 266 nm wavelength [33]. Interestingly, despite the absence of KOH formation in the case of the KCl+Cr mixture, the formed atomic potassium and/or atomic chlorine did interact in the gas phase with gaseous potassium species, which can be seen in the prolonged potassium signal compared to pure KCl (Fig. 3). As shown in Figure 3, the induced fragments react with gas-phase components containing potassium, decreasing the decay rate of free atomic potassium and furthermore, increasing potassium concentration in the gas phase through a slow reaction. Since only the amount of total potassium in the gas phase was measured, the various gaseous species containing potassium could not be identified. In the KCl-induced high-temperature corrosion, KCl is also proposed to play a role similar to a catalyst, meaning it would not be consumed during the reaction [34]. Although not solidly

proven, the longer detection of potassium when studying the KCl+Cr mixture might originate from the decomposition of $K_2CrO_4$, followed by the recombination of KCl.

**Figure 3.** The amount of gaseous potassium as a function of time measured from pure KCl and from a KCl+Cr mixture at 650 °C.

As a summary, the absence of KOH implies that i) KOH did not form in the studied high-temperature reactions; or ii) the formed KOH reacted immediately further to a compound (e.g. $K_2CrO_4$), which could not be detected with the CPFAAS; or iii) the reaction rate was too slow to enable KOH detection with the LOD achieved in this study. However, indications of gas-phase chemistry involving potassium-containing species were observed. Unfortunately, the species could not be identified and further work is required to supplement the missing information.

### 3.2 CI-APi-TOF

A sample spectrum measured by CI-APi-TOF is presented in Figure 4. HCl spectrum can be clearly distinguished from the full spectra because the peaks of the compounds formed in reactions (R4a,b), $Cl^-$ and $HNO_3 \cdot Cl^-$, do not interfere with any other peak. The peaks related to HCl are marked with a green color and the peaks related to $NO_3^-$ ionization and mass calibration are marked with a blue color in the figure. Because chlorine has two stable isotopes, $^{35}Cl$ and $^{37}Cl$, having natural abundances of 76% and 24%, respectively, its peaks are separated to *m*/*z* ratios of 35 Th and 37 Th, of which the height of the first one is about 3-fold compared to the latter one. Similarly, in the case of $HNO_3 \cdot Cl^-$, two separated peaks are seen in *m*/*z* ratios of 98 Th and 100 Th.

**Figure 4.** Sample spectrum measured by CI-APi-TOF. The green peaks represent compounds related to HCl and the blue peaks represent compound related to nitrate ionization and are also the peaks used in mass calibration. The height of the peaks of $NO_3^-$ and $HNO_3 \cdot NO_3^-$ are about one order of magnitude higher than the shown y-scale and are therefore not shown completely here.

It can be observed from Figure 5 and Table 2 that the location of the peaks and the isotopic pattern represent very well the exact masses of the compounds and correspond to the natural abundance of the isotopes of chlorine. The peaks are not located at the nominal masses due to the mass defect of the compounds. The information on the mass defects provided by a high-resolution mass spectrometer can be used to identify the actual chemical composition. Due to a very good correlation between the measured and the theoretical peak locations, mass defects, and isotopic patterns, it is obvious that the peaks at the masses 35 Th, 37 Th, 98 Th, and 100 Th are caused by HCl. The measured spectrum from HCl was also validated by evaporating HCl vapor from a glass bottle in the front of the inlet of CI-APi-TOF. Additionally, there are no interfering peaks at these masses; thus, the total areas of the peaks can be used to examine the concentrations of the compounds.

**Figure 5.** Closer view on the $Cl^-$ and $HNO_3 \cdot Cl^-$ peaks. The grey lines give the measured signal and the black dashed lines represent the peaks having the exact masses of the compounds. The

areas of the peaks with the isotope of $^{35}Cl$ are fitted using the areas of the measured peaks. The areas of the peaks with the isotope of $^{37}Cl$ originate from the natural abundance of the isotope.

**Table 2.** Identified peaks related to HCl.

The absolute concentrations of HCl cannot be reported due to a lack of concentration calibration of HCl. Therefore, the HCl concentrations are reported here as normalized to the total nitrate ion signal using Equation (2). The normalized HCl signal is based on the equation used in concentration calibration [24], with the exception of a lacking calibration coefficient.

$$\text{Normalized HCl signal} = \frac{Cl^- + HNO_3 \cdot Cl^-}{NO_3^- + HNO_3 \cdot NO_3^-} \quad (2)$$

Assuming kinetically limited reactions, which have the same reaction rate constant as with $H_2SO_4$, the concentrations of HCl measured could be approximated to be in ppt level. This level is the same as the minimum detectable level of cavity ring-down spectroscopy. Nevertheless, the possibility of detecting HCl concentrations at a significantly lower level, e.g. at the ppq level, with 1 s time resolution exists with CI-APi-TOF.

As expected, no HCl formed under dry conditions at 550 °C, when solely KCl was studied (Fig. 6). Interestingly, HCl was identified under humid conditions (Fig. 6). In contrast, no KOH was detected with CPFAAS when KCl was studied under the same conditions, as would be expected from Reaction (R5). The reason for no signals of KOH in the gaseous phase might be that it is rather in the liquid state than in the gaseous state under conditions studied. Formation of liquid KOH is supported by the reported calculations according to which KOH(g) is stable at 550 °C only as long as the K(g)/Cl(g) ratio in the gas phase is higher than one [8]. According to Reaction (R5), increasing water vapor content increases the concentration of KOH. However, the increase of water vapor content in the gas phase did not change the measured concentration of HCl dramatically, since the strong thermodynamic stability of gaseous KCl does not favor KOH formation.

$$KCl(g,s) + H_2O(g) \leftrightarrow KOH(g,l) + HCl(g) \quad (R5)$$

The HCl concentrations measured during the reaction between KCl and iron, chromium, or 316L steel were at the same level (Fig. 6). However, the measured concentration when only KCl was exposed to humid conditions was roughly twice as high (Figure 6). This could originate from formation of metal chlorides ($CrCl_x$ and $FeCl_x$), which consume part of the available chlorine, making it unavailable for HCl formation. The instantaneous increase of HCl signals with virtually no time delay at the beginning of water vapor introduction evidenced the high sensitivity and short response time of CI-APi-TOF in the performed gas-phase studies.

**Figure 6.** Normalized HCl signals measured at 550 °C with CI-APi-TOF as functions of measurement time with average HCl concentrations under dry (darker bar plots) and 20 vol % $H_2O$ (lighter bar plots) conditions.

The oxygen concentration of the gas phase did not have any marked effect on the measured concentrations of HCl in any of the studied mixtures (Fig. 7). All the measured HCl concentrations were at the same level as the HCl concentrations measured in the presence of 20 vol.% and 30 vol.% $H_2O$. This indicates that at least a part of the detected HCl formed without oxidation taking place. The presence of oxygen is essential for the formation of metal oxides or oxide-containing intermediates such as $K_2CrO_4$ or $K_2Fe_2O_4$. However, the measured relatively stable HCl concentrations implied that potassium and chlorine may react irrespective of one another with the studied metals. It is worth reminding that the detected concentrations were high enough to qualitatively verify HCl in the gaseous phase, but due to the lack of calibration, accurate quantification of formed HCl could not be carried out.

**Figure 7.** Normalized HCl signals measured at 550 °C with CI-APi-TOF as functions of measurement time with average HCl concentrations for three mixtures in 0-20 vol.% $O_2$ + 30 vol.% $H_2O$.

## 4 Conclusions

High-temperature corrosion reactions between KCl and various metals were studied online by using two different analytical approaches: collinear photofragmentation and atomic absorption spectroscopy (CPFAAS) and chemical ionization atmospheric pressure interface time-of-flight mass spectrometer (CI-APi-TOF). The experiments were carried out at 550 °C under varying gas-phase conditions. The main conclusions of the study can be summarized as follows:

- KOH could not be verified in the gaseous phase in any of the performed measurements. This could result from KOH not being gaseous in the studied temperature range; from the gaseous KOH reacting immediately further; or from a slow formation rate of gaseous KOH.
- CI-APi-TOF proved to be applicable for high-temperature corrosion studies.
- The formation of HCl under humid conditions from only KCl and from the studied mixtures was verified.
- Within the detection resolution, the oxygen or the water content did not affect the concentration of HCl in the gaseous phase.

As a result, further information regarding the mechanism of alkali chloride-induced corrosion was gathered. The identification of HCl in the gas phase and $K_2CrO_4$ as a solid intermediate suggest that the reaction proceeds via route presented as Reaction 1b. First, the alloy and its protective oxide react with KCl, forming $K_2CrO_4$, which reacts further to a non-protective oxide.

## Acknowledgments

This work has been carried out within the Academy of Finland project “Novel Approaches to Study Corrosion Mechanisms in High-temperature Industrial Processes” (Decision no. 296435) and Tampere University of Technology Graduate School. The authors are grateful to Prof.

Mikko Sipilä from University of Helsinki for lending the CI-inlet for the APi-TOF and to the tofTools team for providing tools for mass spectrometry analysis. Mr. Tapio Sorvajärvi is gratefully acknowledged for the aid and guidance with some of the measurements.

**((for typesetters: please format the references in the reference list according to the current design style – see e.g. [1, 2]))**

## References


[1] J. M. Johansen, M. Aho, K. Paakkinen, R. Taipale, H. Egsgaard, J. G. Jakobsen, F. J. Frandsen, P. Glarborg, *Proceedings of the Combustion Institute* **2013**, *34*, 2363.

[2] H. Miettinen-Westberg, M. Byström, B. Leckner, *Energy & Fuels* **2003**, *17*, 18.

[3] Lehmusto, J., Skrifvars, B.-J., Yrjas, P., Hupa, M., Comparison of potassium chloride and potassium carbonate with respect to their tendency to cause high temperature corrosion of stainless 304L steel, *Fuel Processing Technology* **105** (2013), 98-105.

[4] Montgomery, M., Karlsson, A., Larsen, O.H., Field test corrosion experiments in Denmark with biomass fuels, Part 1: Straw-firing, *Materials and Corrosion* **53**(2) (2002), 121-131.

[5] Lehmusto, J., Lindberg, D., Yrjas, P., Skrifvars, B.-J., Hupa, M., Thermogravimetric studies of high temperature reactions between potassium salts and chromium, *Corrosion Science* **59** (2012), 55-62.

[6] Karlsson, S., Pettersson, J., Johansson, L.-G., Svensson, J.-E., Alkali Induced High Temperature Corrosion of Stainless Steel: The Influence of NaCl, KCl and $CaCl_2$, *Oxidation of Metals* **78**(1-2) (2012), 83-102.

[7] Barin, I., *Thermodynamic Data of Pure Substances, 3rd Ed.*, **1995**, VCH, New York, USA.

[8] Blomberg, T., A thermodynamic study of the gaseous potassium chemistry in the convection sections of biomass fired boilers, *Materials and Corrosion* **62**(7) (2010), 635-641.

[9] Folkeson, N., Jonsson, T., Halvarsson, M., Johansson, L.-G., Svensson, J.-E., The influence of small amounts of KCl(s) on the high temperature corrosion of a Fe-2.25Cr-1Mo steel at 400 and 500 °C, *Materials and Corrosion* **62**(7) (2010), 606-615.

[10] Goldenstein, C.S., Spearrin, R.M., Jeffries, J.B., Hanson, R.K., Infrared laser-absorption sensing for combustion gases, *Progress in Energy and Combustion Science* **60** (2017), 132-176.

[11] Ma, L., Lei, Q., Capil, T., Hammack, S.D., Carter, C.D., Direct comparison of two-dimensional and three-dimensional laser-induced fluorescence measurements on highly turbulent flames, *Optics letters* **42**(2) (2017), 267-270.

[12] Oldenborg, R.C., Baughcum, S.L., Photofragment fluorescence as an analytical technique: application to gas-phase alkali chlorides, *Analytical Chemistry* **58**(7) (1986), 1430-1436.

[13] Chadwick, B.L., Ashman, R.A., Campisi, A., Crofts, G.J., Godfrey, P.D., Griffin, P.G., Morrison, R.J.S., Development of techniques for monitoring gas-phase sodium species formed during coal combustion and gasification, *International Journal of Coal Geology* **32**(1-4) (1996), 241-253.

[14] Leffler, T., Brackmann, C., Aldén, M., Li, Z., Laser-induced photofragmentation fluorescence imaging of alkali compounds in flames, *Applied Spectroscopy* **71**(6) (2017), 1289-1299.

[15] Forsberg, C., Broström, M., Backman, R., Edvardsson, E., Badiei, S., Berg, M., Kassman, H., Principle, calibration, and application of the in situ alkali chloride monitor, *Review of Scientific Instruments* **80**(2) (2009), 023104.
[16] Leffler, T., Brackmann, C., Weng, W., Gao, Q., Aldén, M., Li, Z., Experimental investigations of potassium chemistry in premixed flames, *Fuel* **203** (2017), 802-810.
[17] Leffler, T., Brackmann, C., Berg, M., Aldén, M., Li, Z., Online Alkali Measurement during Oxy-fuel Combustion, *Energy Procedia* **120** (2017), 365-372.
[18] Weng, W., Leffler, T., Brackmann, C., Aldén, M., Li, Z., Spectrally Resolved UV Absorption Cross-Sections of Alkali Hydroxides and Chlorides Measured in Hot Flue Gases, *Applied Spectroscopy* **72**(9) (2018), 1388-1395.
[19] Sorvajärvi, T., Saarela, J., Toivonen, J., Optical detection of potassium chloride vapor using collinear photofragmentation and atomic absorption spectroscopy, *Optics Letters* **37**(19) (2012), 4011-4013.
[20] Sorvajärvi, T., DeMartini, N., Rossi, J., Toivonen, J., In situ measurement technique for simultaneous detection of K, KCl, and KOH vapors released during combustion of solid biomass fuel in a single particle reactor, *Applied Spectroscopy* **68**(2) (2014), 179-184.
[21] Hagen, C.L., Lee, B.C., Franka, I.S., Rath, J.L., VandenBoer, T.C., Roberts, J.M., Brown, S.S., Yalin, A.P., Cavity ring-down spectroscopy sensor for detection of hydrogen chloride, *Atmospheric Measurement Techniques*, **7**(2) (2014) 345-357.
[22] Veres, P., Roberts, J.M., Warneke, C., Welsh-Bon, D., Zahniser, M., Herndon, S., Fall, R., de Gouw, J., Development of negative-ion proton-transfer chemical-ionization mass spectrometry (NI-PT-CIMS) for the measurement of gas-phase organic acids in the atmosphere, *International Journal of Mass Spectrometry* **274**(1-3) (2008), 48-55.
[23] Kim, S., Huey, L.G., Stickel, R.E., Pierce, R.B., Chen, G., Avery, M.A., Dibb, J.E., Diskin, G.S., Sachse, G.W., McNaughton, C.S., Clarke, A.D., Anderson, B.E., Blake, D.R., Airborne measurements of HCl from the marine boundary layer to the lower stratosphere over the North Pacific Ocean during INTEX-B, *Atmospheric Chemistry and Physics Discussions* **8** (2008), 3563-3595.
[24] Jokinen, T., Sipilä, M., Junninen, H., Ehn, M., Lönn, G., Hakala, J., Petäjä, T., Mauldin III, R.L., Kulmala, M., Worsnop, D.R., Atmospheric sulphuric acid and neutral cluster measurements using CI-APi-TOF, *Atmospheric Chemistry and Physics* **12**(9) (2012), 4117-4125.
[25] Junninen, H., Ehn, M., Petäjä, T., Luosujärvi, L., Kotiaho, T., Kostiainen, R., Rohner, U., Gonin, M., Fuhrer, K., Kulmala, M., Worsnop, D.R., A high-resolution mass spectrometer to measure atmospheric ion composition, *Atmospheric Measurement Techniques* **3**(4) (2010), 1039-1053.
[26] Eisele, F.L., Tanner, D.J., Measurement of the gas phase concentration of $H_2SO_4$ and methane sulfonic acid and estimates of $H_2SO_4$ production and loss in the atmosphere, *Journal of Geophysical Research: Atmospheres* **98**(D5) (1993), 9001–9010.
[27] Kürten, A., Rondo, L., Ehrhart, S., Curtius J., Calibration of a Chemical Ionization Mass Spectrometer for the Measurement of Gaseous Sulfuric Acid, *Journal of Physical Chemistry A* **116**(24) (2012), 6375-6386.
[28] Sorvajärvi, T., Toivonen, J., Principles and calibration of collinear photofragmentation and atomic absorption spectroscopy, *Applied Physics B* **115**(4) (2014), 533-539.

[29] Yaws, C.L., *Handbook of vapor pressure, Vol. 4: Inorganic compounds and elements*, **1995**, Gulf Publishing, Houston, Texas, USA.
[30] X. Wei, U. Schnell, K.R.G. Hein, Behaviour of gaseous chlorine and alkali metals during biomass thermal utilization, *Fuel* **84** (2005), 841-848.
[31] Lehmusto, J., Lindberg, D., Yrjas, P., Skrifvars, B.-J., Hupa, M., Thermogravimetric studies of high temperature reactions between potassium salts and chromium, *Corrosion Science* **59** (2012), 55-62.
[32] Folkeson, N., Jonsson, T., Halvarsson, Johansson, L.-G., M., Svensson, J.-E., The influence of small amounts of KCl(s) on the high temperature corrosion of a Fe-2.25Cr-1Mo steel at 400 and 500 °C, *Materials and Corrosion* **62**(7) (2010), 606-615.
[33] Sorvajärvi, T., Viljanen, J., Toivonen, J., Marshall, P., Glarborg, P., Rate constant and thermochemistry for $K + O_2 + N_2 = KO_2 + N_2$, *The Journal of Physical Chemistry A* **199**(14) (2015), 3329-3336.
[34] Shinata, Y., Accelerated oxidation rate of chromium induced by sodium chloride, *Oxidation of Metals* **27**(5-6) (1987), 315-332.

**Table 1.** Experiments carried out in the present study.

| **CPFAAS** | | |
|---|---|---|
| Sample | Atmosphere | Temperature [°C] |
| KCl | *Dry*; $N_2$ + 0, 1, 5, 10, or 20 vol.% $O_2$ | 550; 650; 750 |
| KCl | *Humid*; $N_2$ + 30 vol.% $H_2O$ + 0, 1, 5, 10, or 20 vol.% $O_2$ | 550; 650; 750 |
| KCl+Cr | *Dry*; $N_2$ + 0, 1, 5, 10, or 20 vol.% $O_2$ | 550; 650; 750 |
| KCl+Cr | *Humid*; $N_2$ + 30 vol.% $H_2O$ + 0, 1, 5, 10, or 20 vol.% $O_2$ | 550; 650; 750 |
| **CI-APi-TOF** | | |
| KCl | *Dry*; $N_2$ + 20 vol.% $O_2$ | 550 |
| KCl | *Humid*; $N_2$ + 20 vol.% $O_2$ + 10, 20, or 30 vol.% $H_2O$ | 550 |
| KCl+Cr | *Humid*; $N_2$ + 30 vol.% $H_2O$ + 0, 1, 5, 10, or 20 vol.% $O_2$ | 550 |
| KCl+Fe | *Humid*; $N_2$ + 30 vol.% $H_2O$ + 0, 1, 5, 10, or 20 vol.% $O_2$ | 550 |
| KCl+316L | *Humid*; $N_2$ + 30 vol.% $H_2O$ + 0, 1, 5, 10, or 20 vol.% $O_2$ | 550 |

**Table 2.** Identified peaks related to HCl.

| Measured ion | Nominal mass (Th) | Exact mass (Th) | Mass defect (Th) | Measured mass range (Th) | Measured mass defect range (Th) | Difference between measured and exact masses ($10^{-6}$ Th/Th) | Natural abundance of the isotope (%) |
|---|---|---|---|---|---|---|---|
| $^{35}Cl^-$ | 35 | 34.9694 | -0.0306 | 34.9694 … 34.9700 | -0.0306 … -0.0300 | 0 … 17 | 75.78 |
| $^{37}Cl^-$ | 37 | 36.9665 | -0.0335 | 36.9667 … 36.9688 | -0.0333 … -0.0312 | 5 … 62 | 24.22 |
| $HNO_3 \cdot {}^{35}Cl^-$ | 98 | 97.9650 | -0.0350 | 97.9648 … 97.9688 | -0.0352 … -0.0312 | -2 … 39 | 74.94 |
| $HNO_3 \cdot {}^{37}Cl^-$ | 100 | 99.9621 | -0.0379 | 99.9615 … 99.9635 | -0.0385 … -0.0365 | -6 … 14 | 23.95 |

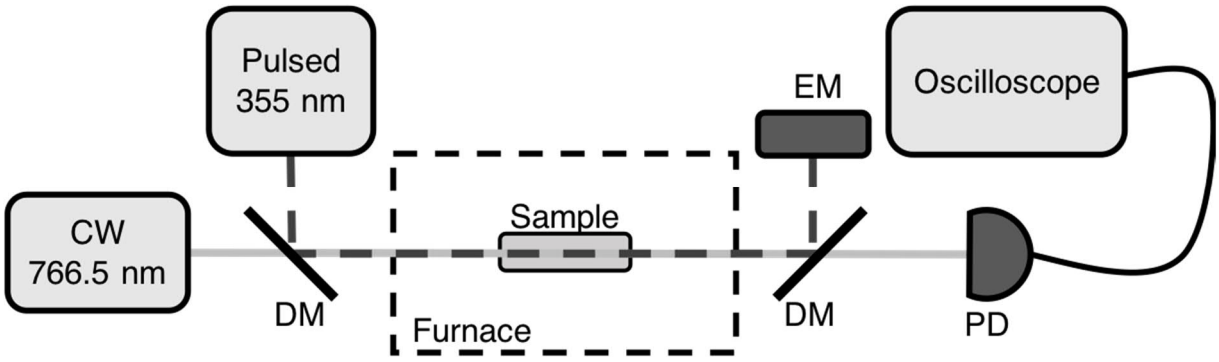


**Figure 1.** A schematic representation of the CPFAAS measurement arrangement used for KOH detection: dichroic mirror, DM; energy meter, EM; photodetector, PD.

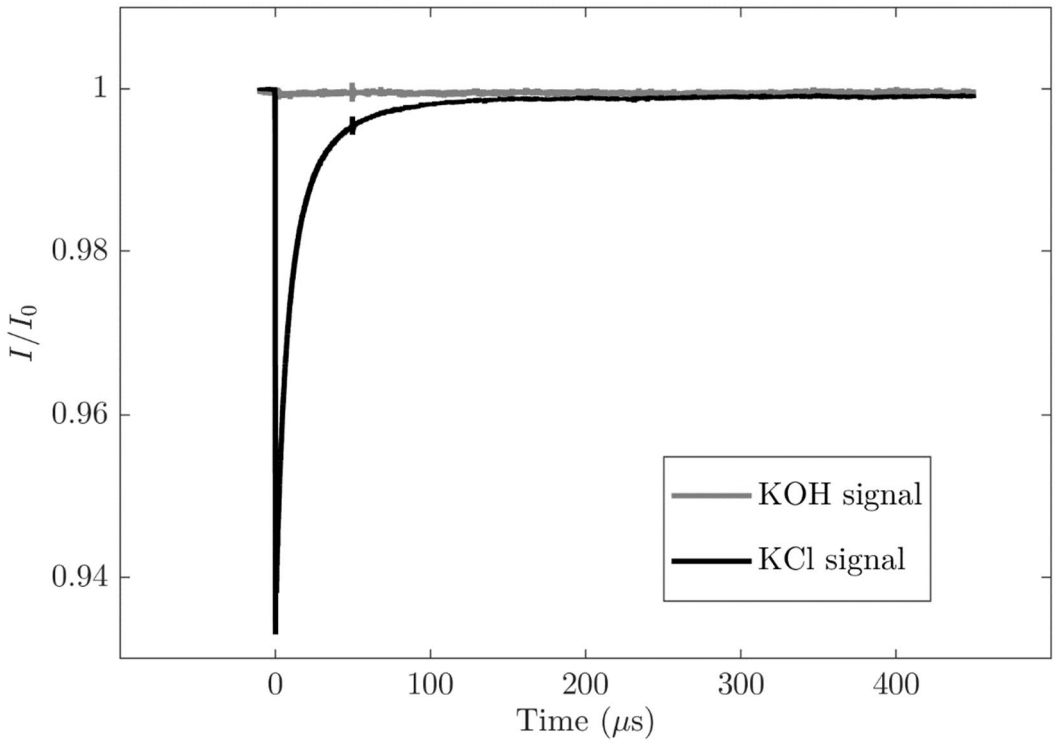


**Figure 2.** A typical signal obtained during corrosion reaction (gray line). The KOH signal was collected when a KCl+Cr mixture was exposed at 650 °C in the presence of 30 vol.% water vapor. As a comparison, a typical KCl signal collected with 120 μJ fragmenting laser pulse energy is also presented (black line). The KCl signal was measured from a pure KCl sample exposed under dry conditions at 750 °C in $N_2$.

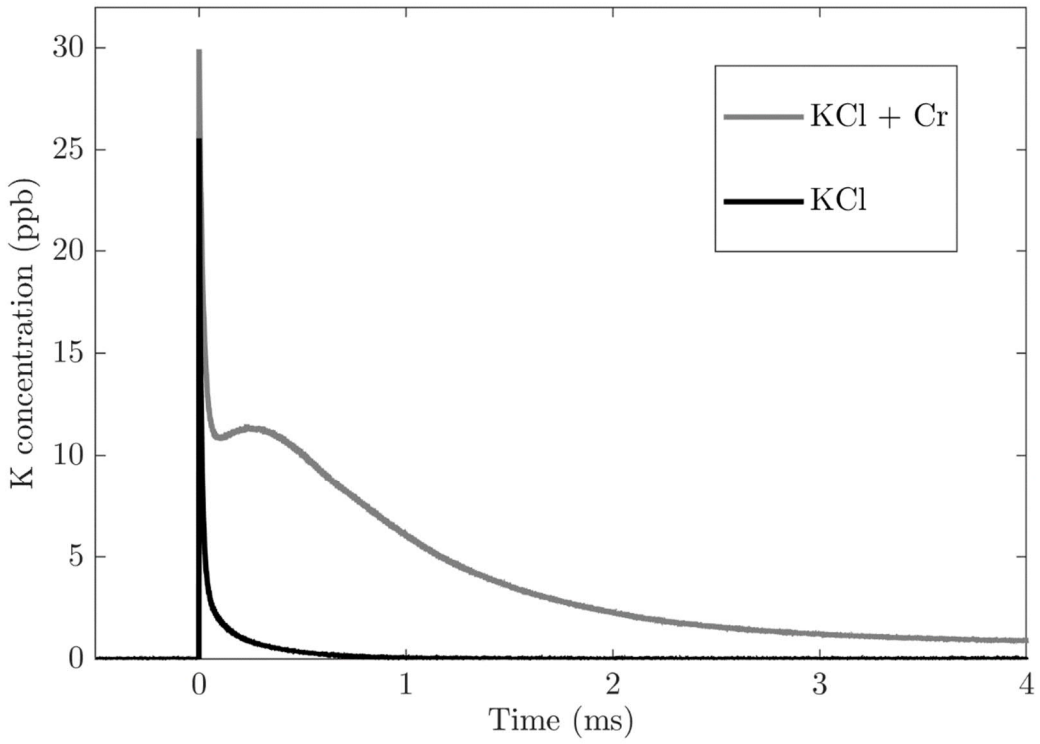


**Figure 3.** The amount of gaseous potassium as a function of time measured from pure KCl and from a KCl+Cr mixture at 650 °C.

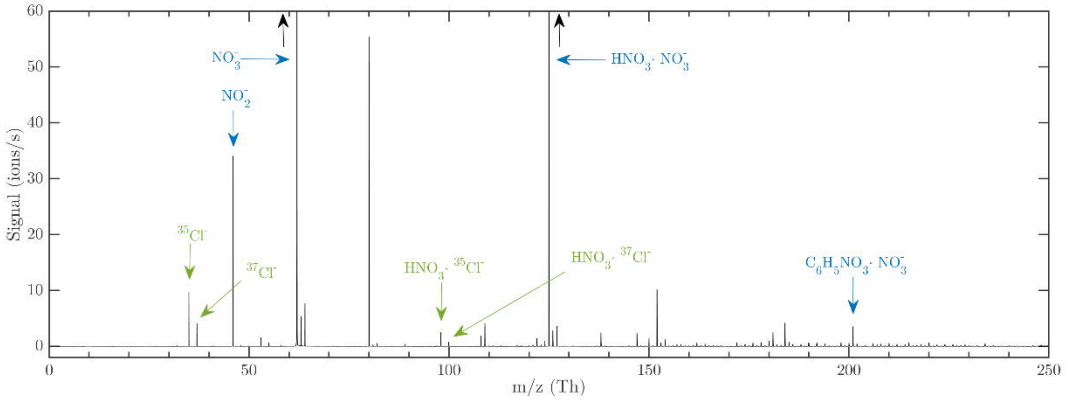


**Figure 4.** Sample spectrum measured by CI-APi-TOF. The green peaks represent compounds related to HCl and the blue peaks represent compound related to nitrate ionization and are also the peaks used in mass calibration. The height of the peaks of $NO_3^-$ and $HNO_3 \cdot NO_3^-$ are about one order of magnitude higher than the shown y-scale and are therefore not shown completely here.

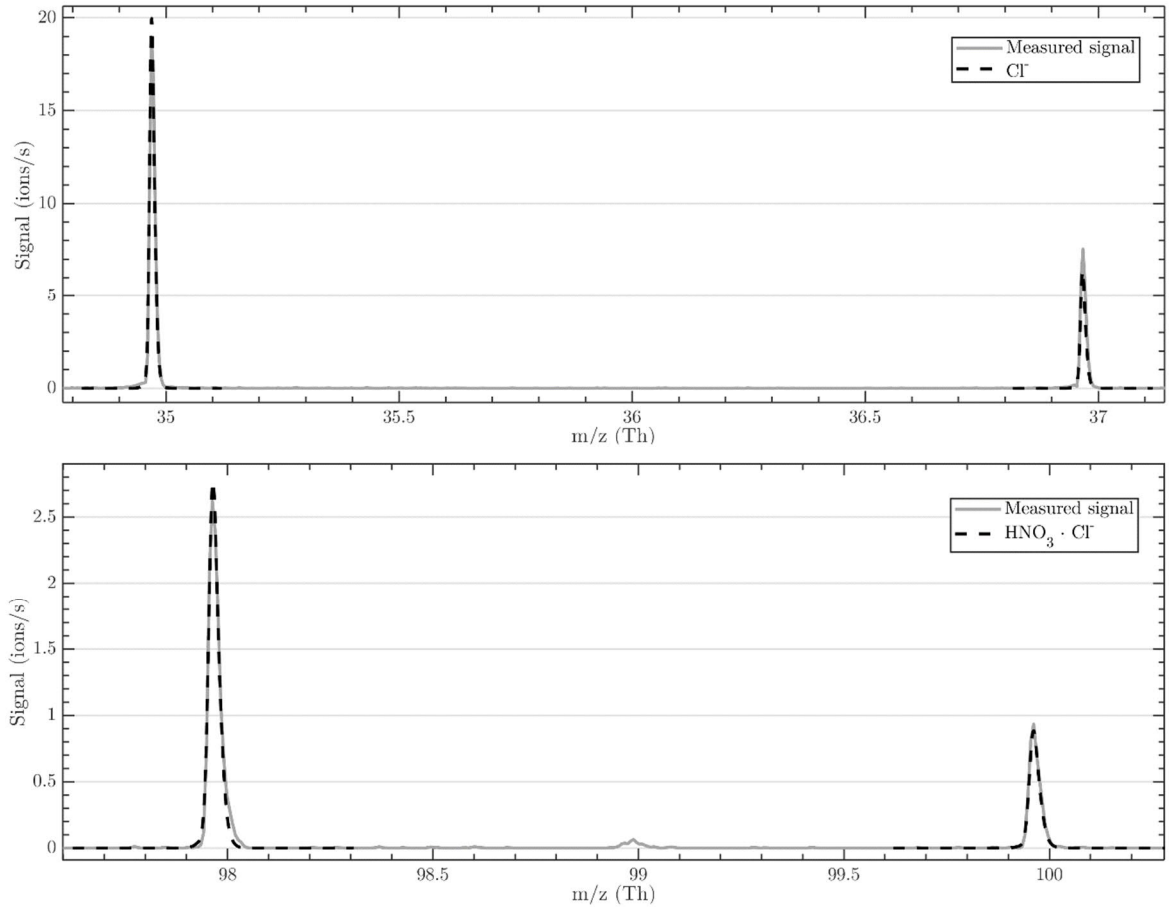


**Figure 5.** Closer view on the $Cl^-$ and $HNO_3 \cdot Cl^-$ peaks. The grey lines give the measured signal and the black dashed lines represent the peaks having the exact masses of the compounds. The areas of the peaks with the isotope of $^{35}Cl$ are fitted using the areas of the measured peaks. The areas of the peaks with the isotope of $^{37}Cl$ originate from the natural abundance of the isotope.

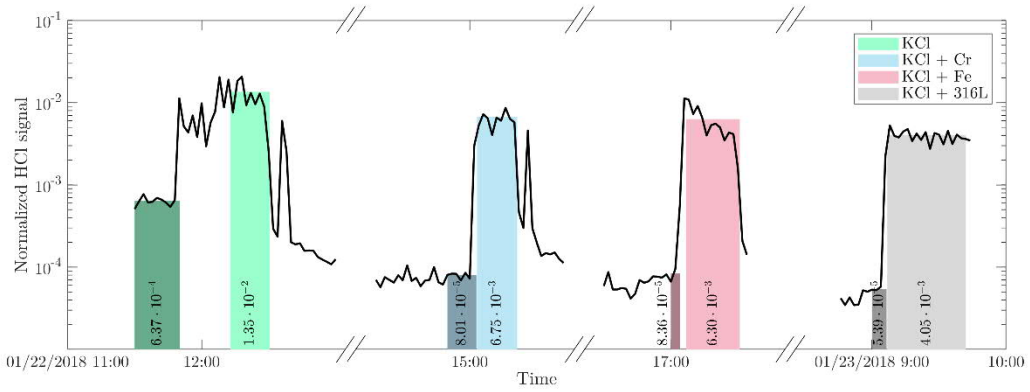


**Figure 6.** Normalized HCl signals measured at 550 °C with CI-APi-TOF as functions of measurement time with average HCl concentrations under dry (darker bar plots) and 20 vol % $H_2O$ (lighter bar plots) conditions.

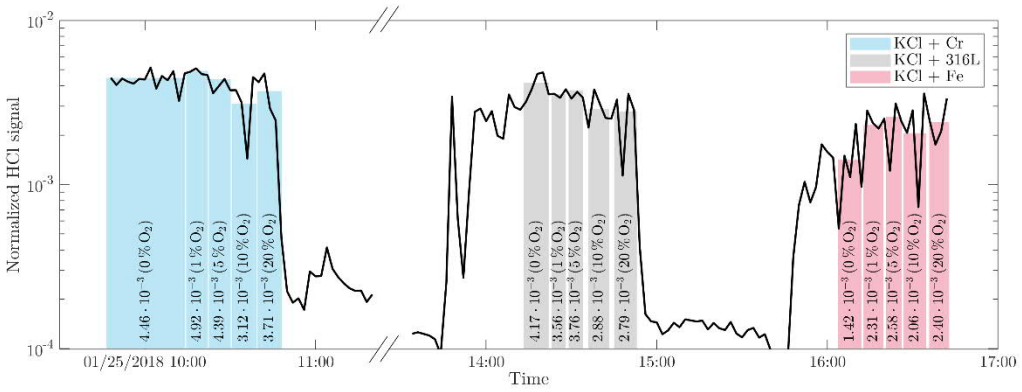


**Figure 7.** Normalized HCl signals measured at 550 °C with CI-APi-TOF as functions of measurement time with average HCl concentrations for three mixtures in 0-20 vol.% $O_2$ + 30 vol.% $H_2O$.